FRET-Based Calcium Imaging: A Tool for High-Throughput/Content Phenotypic Drug Screening in Alzheimer Disease

Kamran Honarnejad[1,2,3]*, Achim K. Kirsch[4], Alexander Daschner[1,2], Aleksandra Szybinska[5], Jacek Kuznicki[5], and Jochen Herms[1,2,6]

Abstract

Perturbed intracellular store calcium homeostasis is suggested to play a major role in the pathophysiology of Alzheimer disease (AD). A number of mechanisms have been suggested to underlie the impairment of endoplasmic reticulum calcium homeostasis associated with familial AD-linked presenilin 1 mutations (FAD-PS1). Without aiming at specifically targeting any of those pathophysiological mechanisms in particular, we rather performed a high-throughput phenotypic screen to identify compounds that can reverse the exaggerated agonist-evoked endoplasmic reticulum calcium release phenotype in HEK293 cells expressing FAD-PS1. For that purpose, we developed a fully automated high-throughput calcium imaging assay using a fluorescence resonance energy transfer–based calcium indicator at single-cell resolution. This novel robust assay offers a number of advantages compared with the conventional calcium measurement screening technologies. The assay was employed in a large-scale screen with a library of diverse compounds comprising 20,000 low-molecular-weight molecules, which resulted in the identification of 52 primary hits and 4 lead structures. In a secondary assay, several hits were found to alter the amyloid β (Aβ) production. In view of the recent failure of AD drug candidates identified by target-based approaches, such a phenotypic drug discovery paradigm may present an attractive alternative for the identification of novel AD therapeutics.

Introduction

Alzheimer disease (AD) is the most frequent form of dementia in the elderly without an effective disease-modifying therapy.[1] Accumulation of extracellular plaques of β-amyloid (Aβ) protein and intracellular neurofibrillary tangles of hyperphosphorylated tau protein in brain are the major pathological AD hallmarks and, in accordance, the main drug targets for AD drug development today.[1] Nevertheless, dysregulated intracellular calcium homeostasis is proposed as an early key event in AD pathogenesis that underlies the disease hallmarks and associated cognitive deficits.[2–5] In fact, impaired calcium homeostasis has been shown to trigger and accelerate Aβ and tangle pathologies[6,7] while also mediating synaptic failure and neuron loss.[8,9] Therefore, pharmacological reversal of calcium dyshomeostasis potentially represents an alternative viable approach for AD therapy. Hence, we aimed at stabilizing intracellular store calcium homeostasis, particularly in the endoplasmic reticulum (ER), as an innovative target for AD drug discovery. To that end, we developed a high-throughput calcium imaging assay, screened a library of 20,000 small molecules, and identified four lead structures that reversed the familial AD-linked mutant presenilin 1 (FAD-PS1)–mediated impairment of ER calcium homeostasis.

[1]Department of Translational Brain Research, DZNE–German Center for Neurodegenerative Diseases, Munich, Germany
[2]Center for Neuropathology and Prion Research, Ludwig Maximilian University, Munich, Germany
[3]Graduate School of Systemic Neurosciences, Ludwig Maximilian University, Munich, Germany
[4]PerkinElmer Cellular Technologies Germany GmbH, Hamburg, Germany
[5]Laboratory of Neurodegeneration, International Institute of Molecular and Cell Biology, Warsaw, Poland
[6]Munich Cluster for Systems Neurology (SyNergy), Munich, Germany
*Current address: Institute of Pharmacology and Toxicology, University of Bonn, Germany

Corresponding Authors:
Kamran Honarnejad, Institute of Pharmacology and Toxicology, University of Bonn, Sigmund-Freud-Straße 25, 53127 Bonn, Germany.
Email: Kamran.Honarnejad@uni-bonn.de

Jochen Herms, Deutsches Zentrum für Neurodegenerative Erkrankungen e.V. München, Ludwig-Maximilians-Universität München, Zentrum für Neuropathologie und Prionforschung, Feodor-Lynen-Straße 23, 81377 München, Germany.
Email: Jochen.Herms@med.uni-muenchen.de

Materials and Methods

Cell Culture and Cell Lines

Human embryonic kidney 293 (HEK293) cells were cultured as previously described.[10] The PS1 lines were then stably transfected with YC3.6/pcDNA3 construct (kindly provided by Dr. A. Miyawaki), and clones were respectively isolated by G418 antibiotic resistance.[11] The HEK293 APPsw/PS1-M146L line was kindly provided by Dr. H. Steiner and cultured as previously described.[12]

Compound Library

DIVERSet 1 and 2 libraries (ChemBridge Corp., San Diego, CA), each containing a diverse collection of 10,000 hand-synthesized small molecules (in total 20,000 compounds), were used for high-throughput compound screening. Compounds fulfilled the "Lipinski's rule of 5," indicating their high druglikeness potential.[13]

High-Throughput Calcium Imaging Assay

For the primary screen, HEK293 cells stably expressing PS1-M146L and Yellow Cameleon 3.6 (YC3.6) were seeded at 13,000 cells/well in 40 μL of growth medium on collagen-coated 384-well CellCarrier plates (PerkinElmer, Rodgau, Germany). After 6 h, using an automated pipetting robot (Bravo; Agilent Technologies, Santa Clara, CA), library compounds were added to each well at the final concentration of 10 μM in 1% DMSO, each in four replicates. All plates contained Thapsigargin (TP; 1 μM; Calbiochem, Darmstadt, Germany), cyclopiazonic acid (CPA; 20 μM; Calbiochem), and 3,4,5-trimethoxybenzoic acid 8-(diethylamino)octyl ester (TMB-8; 50 μM; Sigma-Aldrich, Taufkirchen, Germany) as positive controls, as well as untreated and DMSO vehicle-treated wells. After 24 h using the pipetting robot, DRAQ5 (Biostatus Ltd, Leicestershire, UK), a far-red fluorescent nuclear dye, was added to each well at the final concentration of 500 nM. After 2 h, plates were measured for carbachol (CCh)–induced calcium release using the Opera high-throughput confocal imaging platform (PerkinElmer Cellular Technologies GmbH, Hamburg, Germany). Throughout imaging of the entire plate, 37 °C temperature, 5% CO_2, and 90% humidity were maintained in the plate chamber. Using a 442-nm laser, YC3.6 was excited and its cyan fluorescent protein (CFP) and yellow fluorescent protein (YFP) emissions were separated respectively using 483/35-nm and 540/75-nm filters. In addition, using a 640-nm laser, DRAQ5 dye was excited and its emission was collected by a 690/50-nm filter to locate the nuclei. Imaging was performed with a 20× water immersion autofocus objective. The duration of the entire time-lapse calcium imaging for each well was 23.5 s. This was achieved by imaging at a 2.5-s interval resolution prior to dispensing

CCh (for 5 s) to monitor the basal calcium levels. Next, the CCh-induced calcium rise and decay was monitored for 18.5 s after dispensing. Imaging was performed first at a 1-s interval resolution immediately after dispensing (for 5 s) and subsequently at a 2.5-s interval resolution (for 12.5 s). During dispensing, 10 μL CCh (Calbiochem) diluted in Hank's balanced salt solution (HBSS; 10 μM) was injected into each well concurrent with calcium imaging by an automated dispensing unit, which is part of the Opera platform. Imaging was performed sequentially in all 384 wells.

Data Mining

Data mining, clustering, and identification of the lead structures were performed with the Benchware DataMiner software (Tripos, St. Louis, MO).

Cytotoxcity Assay

The cytotoxicity of the compounds was assessed in vitro using the 3-(4,5-dimethylthiazol-2-yl)-2,5-diphenyltetrazolium bromide (MTT) cell proliferation assay kit (Roche Diagnostics GmbH, Mannheim, Germany) according to the manufacturer's instructions and previously described protocols.[14]

Aβ Measurements

Levels of three different Aβ species (Aβ38, Aβ40, and Aβ42) were measured using sandwich enzyme-linked immunosorbent assay (ELISA). Pools of HEK293 cells stably transfected with APPsw/PS1-M146L were used to study the effect of compounds on Aβ generation. According to Page et al.,[12] cells were seeded at a density of 200,000 cells/well in collagen/poly-L-lysine (PLL)–coated 24-well plates and incubated for 24 h in growth medium. Next, the medium was exchanged with 500 μL of fresh medium containing the compounds, the positive control DAPT (10 μM; Calbiochem), or DMSO vehicle. After 16 h, conditioned medium was collected and the levels of secreted Aβ38, Aβ40, and Aβ42 fragments were quantified using the "Human (6E10) Abeta 3-Plex" sandwich ELISA immunoassay kit (Meso Scale Discovery, Rockville, MD) according to the instructions of the manufacturer. The light emission after electrochemical stimulation was measured using the Sector Imager 2400 reader (Meso Scale Discovery). Based on the values generated with calibration standards, corresponding concentrations of Aβ species were calculated using the Meso Scale Discovery Workbench software. All measurements were performed in four replicates.

Statistical Data Analysis

GraphPad Prism 5.0b (GraphPad Software, San Diego, CA) was used for statistical analysis of the data. Values represent

mean ± standard deviation. To test significance, a two-tailed Student *t* test was performed and differences were considered statistically significant if $p < 0.05$.

Results

FRET-Based Calcium Imaging Using YC3.6

YC3.6, a superior genetically encoded fluorescence resonance energy transfer (FRET)–based calcium indicator with predominant cytosolic localization, expanded dynamic range, and fast kinetics,[11] was introduced to HEK293 cells as a tool to monitor both the basal calcium concentrations and the released calcium from ER in real time by confocal imaging. YC3.6 is composed of CFP and YFP domains, linked via calmodulin (CaM) and a CaM-binding peptide (M13). Upon calcium binding, it undergoes a conformational change and thereby FRET efficiency increases (**Fig. 1A**).[11]

The assay readout was the peak response of inositol-1,4,5-trisphosphate receptor (IP_3R)–evoked calcium release from ER. Agonist-induced IP_3 production by CCh results in calcium release from ER (**Fig. 1B**). The release of calcium from ER into the cytosol results in rise of calcium concentration that can be monitored by increased FRET efficiency.

Time-lapse calcium imaging indicates that within a few seconds after dispensing CCh, FRET efficiency rapidly increases—that is, the CFP (FRET donor) signal decreases, while the YFP signal (FRET acceptor) increments (**Fig. 1C,D**, upper panel).

In **Figure 1C**, the acceptor-donor signals of all cells in a single well are shown for two time points. One set of points are single-cell signals before dispensing, and the other set of points are the signals 3 s after dispensing. The slope of the distribution corresponds to the FRET signal, which is calculated as the ratio of the YFP to CFP signal. The change in FRET efficiency after stimulating with CCh is clearly visible in the change of distribution slope (**Fig. 1C**). In accordance, the FRET ratio (YFP/CFP) can be used as a tool to monitor calcium dynamics (**Fig. 1D**, lower panel). Following the rise in calcium concentration, the peak of calcium release is reached. After the peak, the FRET ratio begins to decay as a result of calcium buffering and sequestration (**Fig. 1D**).

FAD-PS1 Mutations Enhance the Amplitude of CCh-Induced Calcium Release and the Number of CCh-Responsive Cells

Mutations in presenilins (PS1 and PS2) account for the vast majority of early onset familial Alzheimer disease (FAD) cases. These mutations result in increased IP_3R sensitivity.[15] Moreover, function of multiple upstream elements of IP_3 receptor-mediated calcium release is also affected in

AD—for example, G-protein–coupled receptors (GPCRs) in general[16] and muscarinic receptors in particular,[17] G-proteins,[18] and phospholipase C (PLC).[19] Presumably, the combination of those results in a remarkably greater IP_3R-mediated calcium release in FAD-PS1 cells. Since the screening hits may potentially target any of those upstream elements, such a phenotypic multitargeted drug screening paradigm allows collectively addressing several aspects of AD.

Indeed, using the developed FRET-based calcium imaging assay, we could confirm the exaggerated CCh-evoked ER calcium release signals in cells expressing different mutant forms of PS1 (**Fig. 1E**). The peak response of CCh-evoked calcium release and the number of CCh-responsive cells were remarkably higher in FAD-PS1 lines (PS1-M146L, PS1-C92S, PS1-DeltaE9) compared with the wild-type PS1 line (**Fig. 1F,G**). Likewise, the expression of a γ-secretase–deficient mutant form of PS1 (PS1-D385N) results in increased responsiveness to CCh and augmented calcium release from ER upon CCh stimulation (**Fig. 1F,G**). To assess the single-cell resolution of the assay, the traces for individual cells showing the raw and normalized FRET ratio changes (CCh-evoked calcium responses) are plotted for cells expressing either wild-type or mutant forms of PS1 (**Suppl. Fig. S1**). By looking at the single-cell traces, particularly in cells expressing wild-type PS1, a large natural variability in peak amplitudes of calcium response is evident (**Suppl. Fig. S1**). This is likely to be caused by the natural lower sensitivity of IP_3R gating at suboptimal concentrations of IP_3 as well as the smaller scale of calcium release in wild-type PS1 versus FAD-PS1 cells.[15]

Therefore, the augmented CCh-evoked calcium release in FAD-PS1–expressing cells was used as a robust phenotypic readout in a high-throughput screening (HTS) approach, which aimed at identification of drugs that can reverse the exaggerated calcium release to physiological levels (**Suppl. Fig. S3A**). Active compounds would affect the latter phenotypic readout by potentially targeting the IP_3R sensitivity, the upstream elements of IP_3R-evoked calcium release (muscarinic receptors, GPCRs, and PLC), or calcium channels and pumps on the ER membrane. Moreover, compounds that directly affect the ER calcium load can also be identified in this screening paradigm. The latter is particularly important, as the ER calcium load is suggested to be altered in the pathophysiology of AD.[3,20]

Assay Development

We addressed intracellular store calcium dyshomeostasis as an innovative target for drug discovery with a novel FRET single-cell–based calcium imaging technique in a fully automated high-throughput kinetic assay on the Opera system (PerkinElmer) for compound screening.
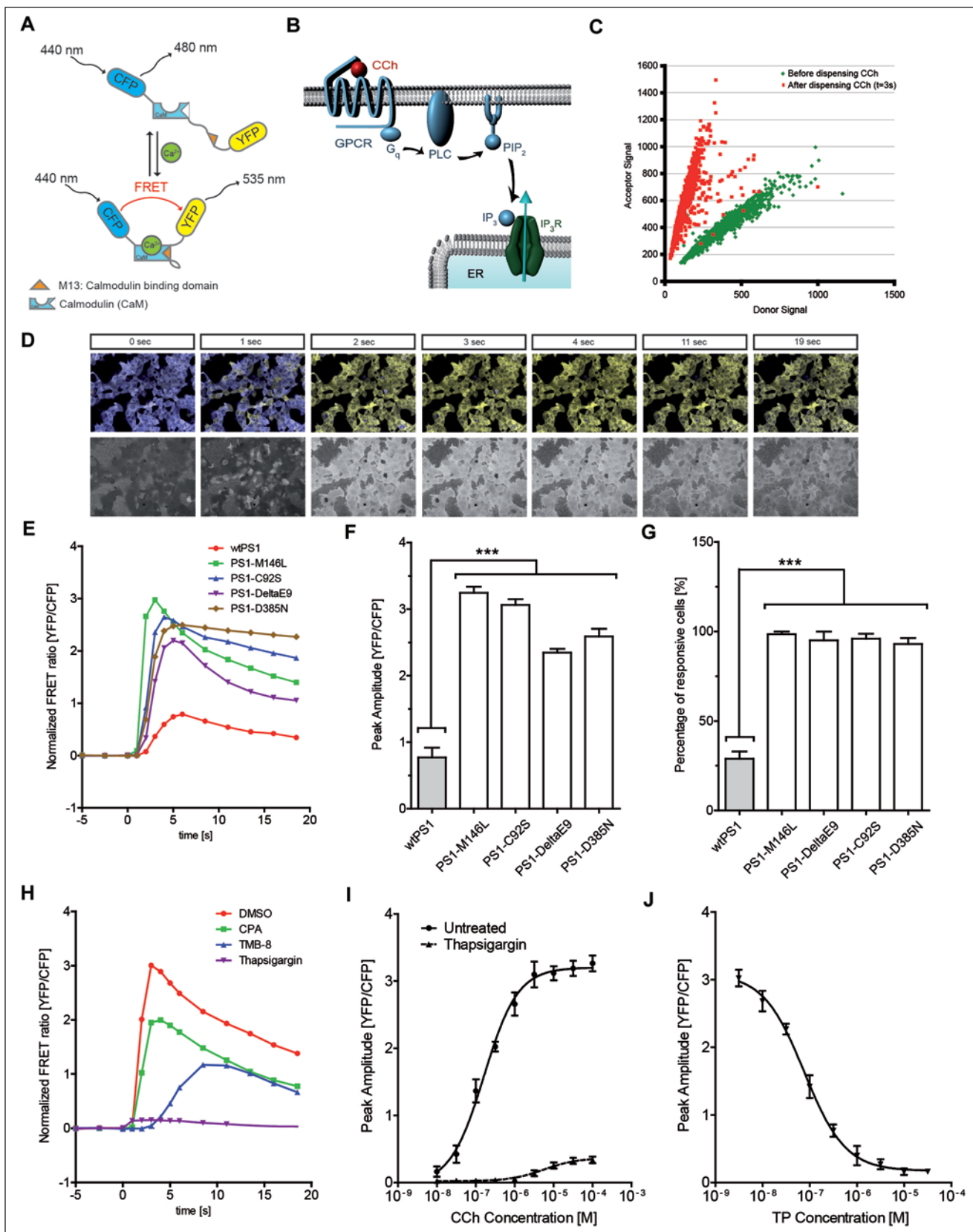
Figure 1. Fluorescence resonance energy transfer (FRET)–based calcium imaging with Yellow Cameleon 3.6 (YC3.6). (**A**) Structure of the calcium sensor YC3.6 that is a fusion protein composed of cyan fluorescent protein (CFP) and yellow fluorescent protein (YFP)

attached via calmodulin (CaM) and a CaM-binding peptide (M13). Calcium binding brings CFP and YFP together, shifting the emission of 480 nm to 535 nm upon excitation at 440 nm. (**B**) Carbachol (CCh) application initiates a pathway, which results in calcium release from the endoplasmic reticulum (ER). CCh exposure leads to G-coupled activation of phospholipase C (PLC), catalyzing the hydrolysis of the membrane-associated PIP_2 molecule to IP_3. Binding of the IP_3 molecule to IP_3 receptor channels (IP_3R) on the ER membrane in turn leads to opening of IP_3R channels and calcium release from the ER to the cytosol. (**C**) FRET acceptor-donor distribution signal before (green) and after (red) dispensing CCh. The slope of the distribution corresponds to the FRET signal, which is calculated as the ratio of the YFP over CFP signal. (**D**) Representative calcium-dependent changes in FRET are shown upon stimulation with CCh. Upper panel shows the merged image of FRET donor (blue) and acceptor (yellow). The lower panel shows the FRET ratio signal in gray scale. (**E**) Representative calcium transients of CCh-evoked calcium release in cells expressing mutant variants versus wild-type presenilin (PS) upon CCh application. (**F**) The average peak amplitude of CCh-induced calcium release is significantly potentiated in familial Alzheimer disease (FAD) and inactive PS1 mutants compared with wild-type PS1 cells (***$p < 0.001$). (**G**) The average number of responsive cells to CCh is remarkably increased in cells expressing FAD and inactive PS1 mutants compared with wild-type PS1 cells (***$p < 0.001$). (**H**) Representative calcium transients of CCh-evoked calcium release in PS1-M146L HEK293 cells treated with carrier DMSO or positive controls cyclopiazonic acid (CPA), 3,4,5-trimethoxybenzoic acid 8-(diethylamino)octyl ester (TMB-8), and thapsigargin (TP). (**I**) Dose-response effect of CCh agonist on the peak amplitude of calcium release in untreated or TP-treated PS1-M146L cells. (**J**) Dose-dependent effects of TP on the peak amplitude of CCh-evoked calcium release in PS1-M146L cells.

The assay readout was the potentiated IP_3R-evoked calcium response in HEK293 cells expressing a FAD-linked mutation, PS1-M146L. Indeed, treatment with three different positive controls (TP, CPA, and TMB-8) resulted in decreased CCh-evoked calcium release from the ER (**Fig. 1H**).

The dose-dependent effect of CCh in increasing the peak amplitude of calcium response was evaluated across a range of different CCh concentrations in PS1-M146L cells (**Fig. 1I**). Indeed, pretreatment with TP lowered the peak amplitude of the ER calcium response in all CCh concentrations tested (**Fig. 1I**). Moreover, the dose-dependent effect of TP in lowering the peak amplitude of CCh-induced calcium release was investigated (CCh: 10 μM) (**Fig. 1J**).

Image Analysis

The image analysis software Acapella (PerkinElmer) was used to convert the time-lapse images into numerical values. Acapella is a scripting-based solution for implementing different requirements on the image analysis side. The image analysis consisted of four steps: segmenting the image into the individual cells, determining the time-dependent signals for each identified cell, processing the signals of each cell, and then classifying cells and reporting relevant results (**Fig. 2A**).

Image segmentation. For the segmentation, the nuclei and CFP images of the first time point were used. The segmentation of the nuclei image was done with the nuclei_detection_B() algorithm of the Acapella, which involves automatic threshold calculations and some masking steps to split nuclei in close proximities along lines of darker pixels. For each detected nucleus (based on DRAQ5 signal), the CFP signal for that time point was also determined. The nuclei with a signal below a certain threshold were excluded from image analysis. In addition, the CFP signal after dispensing CCh was measured to detect and exclude the cells that were washed away in the well due to dispensing.

Starting from the initially segmented nuclei, the cytoplasm_detection_c() algorithm of Acapella was used to determine the location and shape of the cells using the CFP image. Here again, threshold calculations were used by Acapella to define the final cell shape. In addition, we excluded the cells located at the edges of the image (image borders) to minimize the potential of artifacts caused by only partially visible cells.

For the short time series as used in this HTS approach, the motility of the cells can be neglected. We compared the covered areas by the cells when the detection algorithm was applied to the first and a later time point. In **Figure 2B**, the detected cell areas are outlined for time points at $t = -5$ s and at $t = 1$ s (times are relative to the dispensing time). Also shown are the "overlap area" between the two time points, as well as the area that is only detected at $t = -5$ s ("lost area") and at $t = 1$ s ("gained area"). The size of these areas (normalized to the size at $t = -5$ s) is presented over the entire course of time-lapse calcium imaging for PS1-M146L cells (**Fig. 2B**). Similarly, the changes in the overlap, gained, and the lost areas for DMSO- or positive control-treated cells are shown (**Suppl. Fig. S2**). All curves show a predominant change between $t = 0$ s and $t = 1$ s, indicating that dispensing of CCh into the wells may cause a mechanical stress, causing changes in the covered cell areas. However, these changes were often small, as the values for the lost and gained areas were approximately on the order of 4% to 5%. Therefore, we decided to neglect such small area changes within the short period of time-lapse calcium imaging. However, for longer kinetic experiments, it might be necessary to adjust the cell boundaries for each time point.

Measuring signals. As presented in **Figure 1D** (and **Suppl. Videos S1** and **S2**), calcium-dependent changes in FRET are shown upon stimulation with CCh (shown either as the merged image of donor shown in blue and acceptor in yellow or FRET ratio signal in gray scale). In the color images,
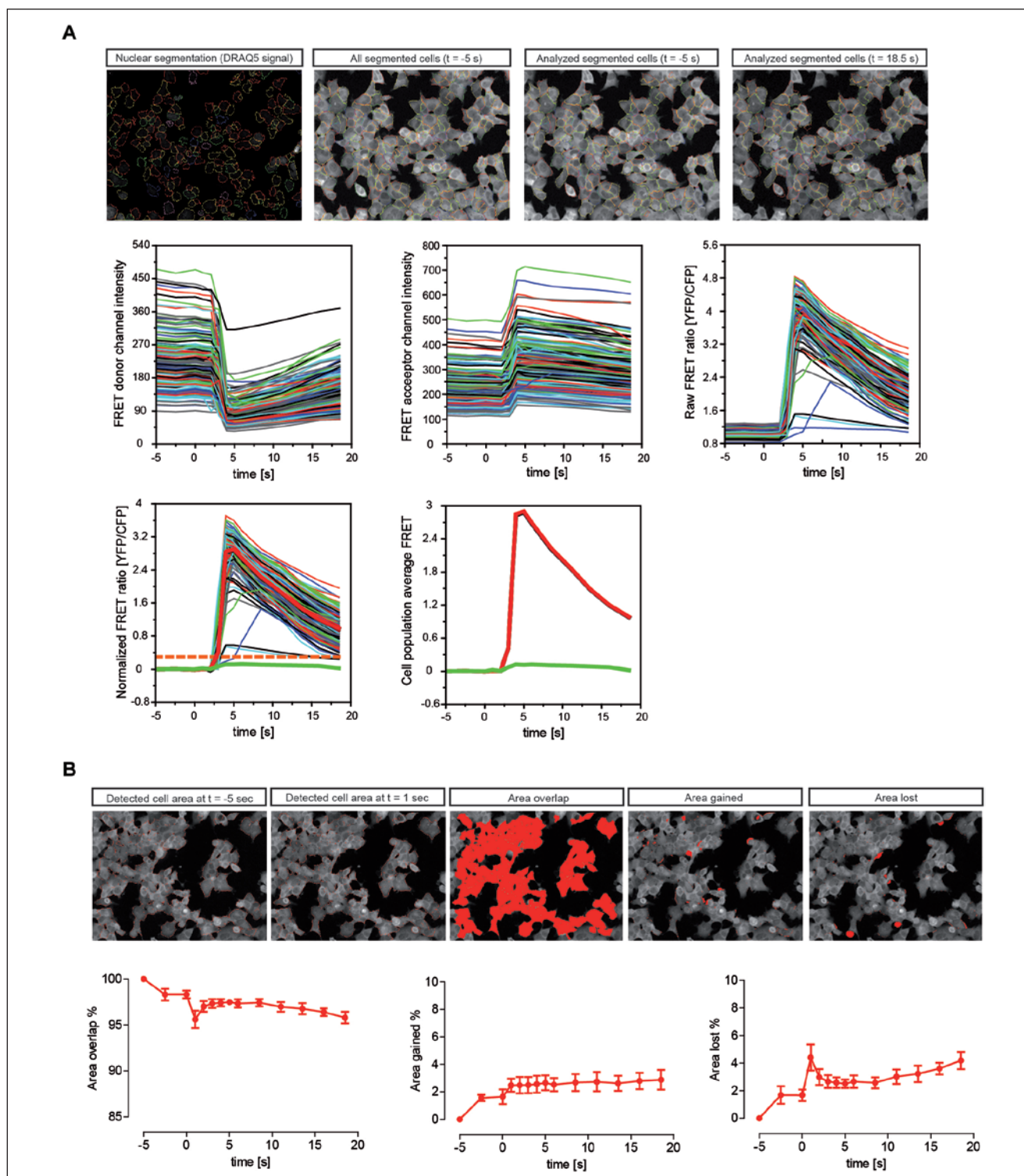
Figure 2. Image analysis workflow and detected cell area change over the course of time-lapse imaging. (**A**) Initially, all the nuclei from the images of the first time point are segmented (based on DRAQ5 signal). For each detected nucleus, the corresponding cyan fluorescent protein (CFP) signals are determined at the first time point. Next, the cells located at the edges of image are excluded. The minimal motility of the cells during the course of imaging is neglected, and the intensity changes inside of the cell areas detected at the first time point are monitored over time (upper panel). Fluorescence resonance energy transfer (FRET) donor, acceptor, raw FRET, normalized FRET, and average FRET response traces to carbachol (CCh; 10 µM) are presented (middle and lower panels). The orange dashed line represents the arbitrarily defined threshold of responsiveness. The red and green curves respectively correspond to the average calcium release of responsive and nonresponsive cells. (**B**) The detected cell areas for time points at $t = -5$ s (first time point) and at $t = 1$ s (after dispensing) are shown. Also shown are overlap, gained, and lost areas between the two time points. The size of overlap, gained, and lost areas (normalized to the size at $t = -5$ s) is presented over the entire course of time-lapse calcium imaging for PS1-M146L cells.

the nuclei are visible as areas of lower fluorescence signal. However, in the FRET ratio images, the nuclei are not clearly visible anymore, indicating that the FRET efficiency is homogeneous throughout the cell body.

Processing the cell signals. For each cell, the average FRET ratio before dispensing was determined as an individual offset value. From the measured FRET signals, this offset was subtracted, so that we obtain the FRET signal changes relative to the predispensing condition. In addition, also the shape of the FRET signal change over time can be evaluated. In particular, both the amplitude of the "maximum" FRET efficiency, as well as the "time" at which this maximum response is reached, can be analyzed.

For example, in the wild-type PS1 cells, after approximately a 6-s delay from dispensing CCh, the peak of FRET response was reached. However, in FAD-PS1 cells, the FRET peak response delay was shorter (depending on the mutation, peak of FRET response was reached within 1–4 s after dispensing CCh) (**Fig. 1E**). In other words, FAD-PS1 mutations enhance the calcium release from the ER, while also shortening the latency of calcium release after dispensing CCh. On the other hand, positive controls CPA and TMB-8 further extended this latency in PS1-M146L cells (**Fig. 1H**).

Classification of cells. For every cell, the maximum increase of the FRET signal and the time point at which this maximum is reached are determined. The cells are classified into responsive and nonresponsive cells based on an arbitrarily defined threshold value and whether the peak FRET value lies below or above that threshold.

High-Throughput Compound Screening Workflow

As illustrated in **Supplemental Figure S4**, HEK293 cells stably coexpressing the FAD-linked PS1-M146L mutation and YC3.6 were seeded on 384-well optical bottom plates. After 6 h, compounds from the library plates were distributed into separate wells by automated pipetting. After 24 h compound incubation, DRAQ5 nuclear marker was added to the wells. After 2 h, time-lapse calcium imaging was performed and CCh-induced calcium release was monitored sequentially for each well using the YC3.6 calcium indicator. In addition, the signal of DRAQ5 dye was also collected throughout the entire course of time-lapse imaging, which was necessary for image analysis. For every detected cell, calcium transients were measured over the course of imaging by calculating and normalizing the YFP/CFP ratios. The peak response amplitude of the calcium rise upon CCh injection was the output of automated analysis at a single-cell level. CCh nonresponsive cells were excluded from the analysis by setting an arbitrarily defined threshold. The

average peak amplitude of all responsive cells in a well was calculated as the final output of the image analysis.

The performance of the high-throughput compound screening assay remained very robust throughout screening of 200 plates (Z′ factor > 0.8). Z′ factors for 10 randomly selected plates are presented in **Supplemental Figure S3B**. The average Z′ factor for those 10 plates was determined to be 0.806 ± 0.029, reflecting the robustness of the assay for HTS.
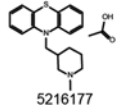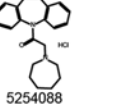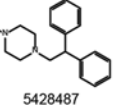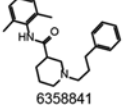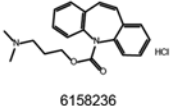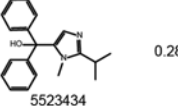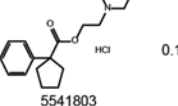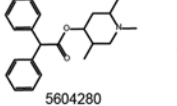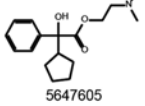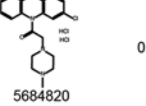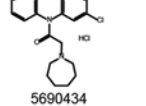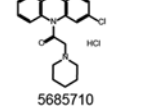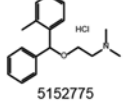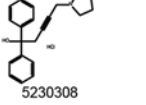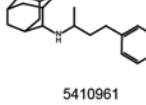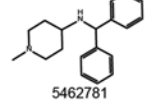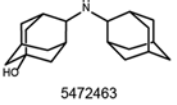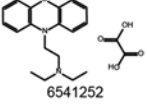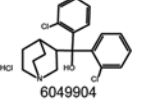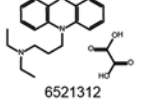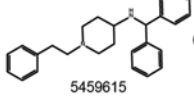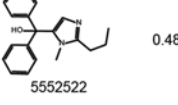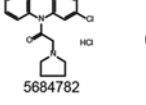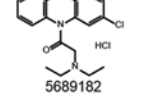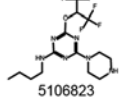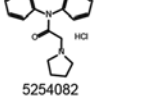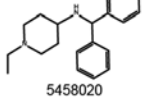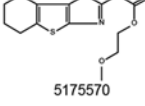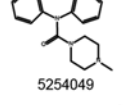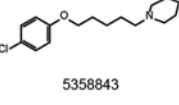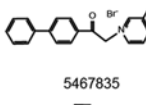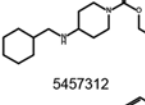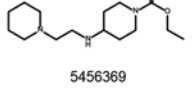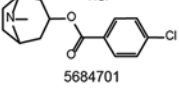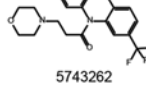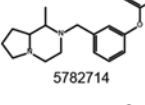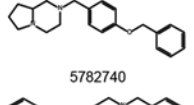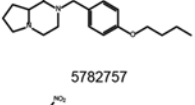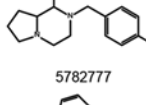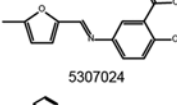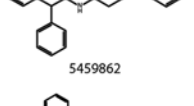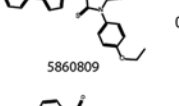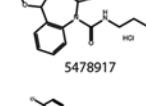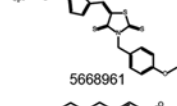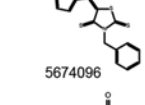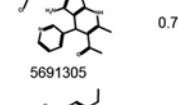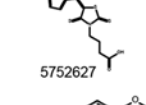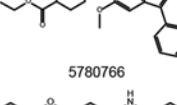
High-Throughput Compound Screening Assay Enables the Discovery of Novel Lead Structures

After filtering the autofluorescent and highly toxic compounds, the primary screen yielded 52 hits (**Fig. 3**). A compound was regarded as a hit if the peak response of calcium release in cells treated with that compound was <90% of that in DMSO-treated controls. To each library compound, a score typically <1.0 was assigned indicating a measure for its efficacy, calculated by dividing the peak response of calcium release in cells treated with that given compound to the peak response of DMSO-treated controls on the same plate. Hereafter, we refer to this value as the "normalized ER calcium response score." In **Figure 3**, a list of all hits from the primary screen, including their chemical structures and corresponding normalized ER calcium response scores, is presented.
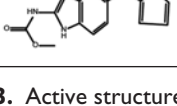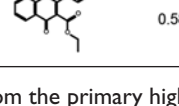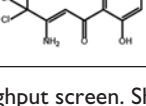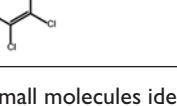
The activity of all primary hits was validated in PS1-M146L cells and confirmed in two other FAD-PS1 lines (PS1-C92S and PS1-DeltaE9) (**Fig. 4A** and **Suppl. Fig. S6**). Fifty-two structures identified from the primary screen were classified into different categories based on their efficacy (**Suppl. Fig. S5**). These categories are separated according to the corresponding values of the normalized ER calcium response score, presented as percentages in relation to the peak response of the DMSO-treated control.

Preliminary structure-activity relationship (SAR) assessments led to the identification of four lead structures. Those structures belonged to the following classes of compounds: thiazolidine, phenothiazine, imidazole, and benzhydrilpiperidinamine (**Suppl. Figs. S7–S11**). A SAR map of the clusters was generated, where clusters with more than 50% active compounds were represented as stars and clusters with less than 50% active compounds as rectangles. In addition, all clusters with more than four active compounds were colored in blue and otherwise in red. The sizes of the symbols correlate directly with the number of compounds in each cluster (**Suppl. Fig. S7**).

In the MTT assay, most hits showed no toxicity. HEK293 cells treated with the hits at 10 µM for 24 h remained viable (**Fig. 4B**). Treatment with only five compounds, three of which belonged to the thiazolidine lead structure, resulted in a 30% to 40% reduction in cellular viability.

Figure 3. Active structures identified from the primary high-throughput screen. Shown are 52 small molecules identified from the primary screen with their chemical structure and the corresponding normalized mean endoplasmic reticulum (ER) calcium response ± standard deviation values generated at 10 µM as a measure for their activity.
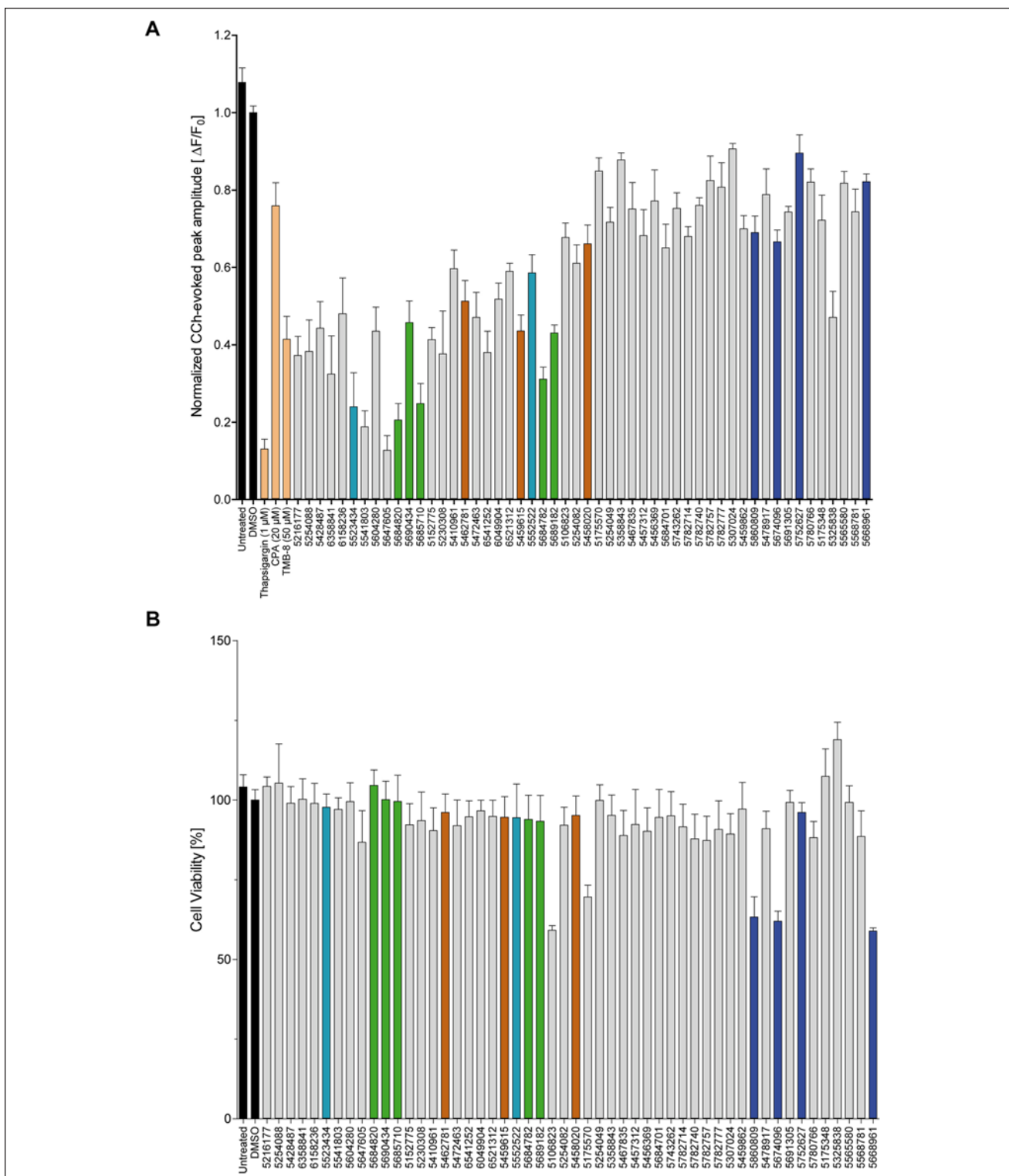
Figure 4. Validation of primary hits and their in vitro cytotoxicity. (**A**) The activity of all 52 primary hits was validated in the PS1-M146L line. All the hits were capable of reducing the peak response of carbachol (CCh)–induced calcium release to <90% of DMSO-treated controls. The peak response of the DMSO-treated control was set to 1. (**B**) Viability of HEK293 cells treated with the primary screen hits was assessed by means of the MTT assay after a 24-h compound treatment. Values are presented as percentage of viable cells. The data for analogous molecules belonging to the same lead structure are marked with the same color.
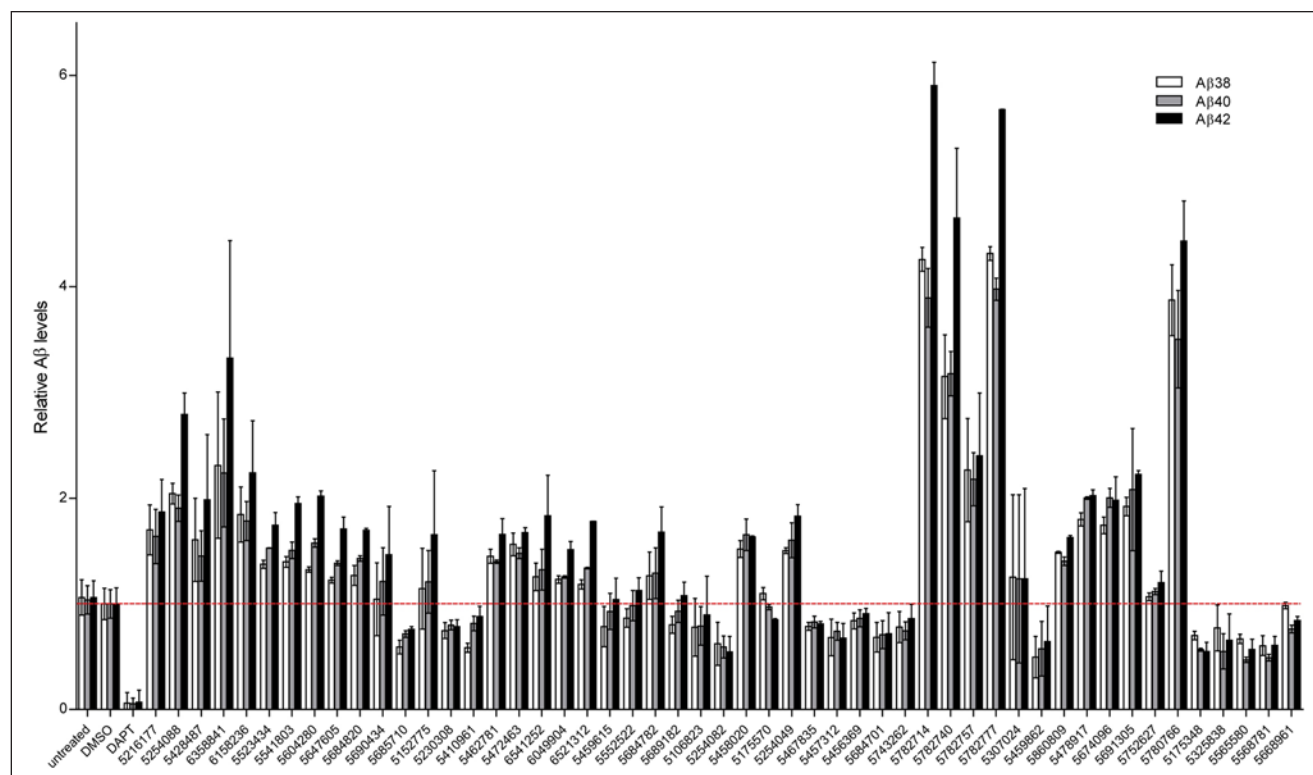
Figure 5. Effects of the active compounds from the calcium high-throughput screening (HTS) on Aβ production. Altered production of Aβ38, Aβ40, and Aβ42 after a 16-h treatment of HEK293 cells coexpressing APPsw and PS1-M146L with the active structures identified from the calcium HTS. DAPT (10 µM) was used as a γ-secretase inhibitor control.

Effect of Hits on Aβ Generation

Modulation of calcium homeostasis affects the production to amyloid β (Aβ) peptide, the major constituent of the amyloid plaques in the AD brain.[6] Furthermore, we also tested the effects of primary screen hits on Aβ peptide production. Depending on the compound tested, we detected increased, decreased, or unchanged Aβ levels upon 16-h exposure of HEK293 APPsw/PS1-M146L cells with the compounds (**Fig. 5**).

Discussion

Here we describe the development and implementation of a high-throughput compound screening assay targeting ER calcium dysregulation as an innovative approach for AD drug discovery. As opposed to the majority of AD drug discovery strategies that target late-stage disease hallmarks, this approach targets a cellular event that is proposed to occur early in the pathophysiology of AD.[2]

Various mechanisms have been proposed to underlie the FAD-PS1–mediated enhancement of the ER calcium release—for example, enhanced IP$_3$ and ryanodine receptor (RyR) channel activities,[15,21] altered sarcoendoplasmic reticulum calcium ATPase (SERCA) pump function,[22] decreased store-operated

calcium entry (SOCE),[23] and loss of PS holoprotein passive calcium leakage.[20] Irrespective as to which of those are the primary causative and which the secondary phenomena, we performed a phenotypic compound screen and identified small molecules that reverse the exaggerated calcium release from ER in cells expressing a FAD-PS1 mutation.

The HTS assay developed offers several advantages compared with current calcium measurement screening technologies. First, the use of genetically encoded calcium sensors as opposed to conventional synthetic calcium-sensitive dyes allows monitoring intracellular calcium dynamics without the drawbacks caused by dye toxicity, loading, washing, and leakage. Second, the developed HTS assay allows performing rapid automated dispensing of reagent jets to individual wells during calcium measurements with no time lag between dispensing and imaging. The latter is ideal for kinetic measurements that require rapid imaging with no delay after dispensing (e.g., fast agonist-induced calcium release). Third and most important, as opposed to single-well–based calcium measurement systems, the single-cell–based nature of this assay in combination with automated image analysis enables simultaneous monitoring of calcium transients in individual cells of a well and applying multiple filtering parameters in image analysis to set apart different cell subpopulations. Furthermore, the assay offers a competitive robustness reflected by a Z′

factor >0.8. An obvious limitation of this assay is, however, the difficulty of calibrating the FRET signals to actual calcium concentrations. Yet for HTS purposes, with a suitable signal window, it is often not necessary to measure the absolute calcium concentrations.

Calcium alterations associated with FAD-PS expression provide ideal means to investigate the disruption of ER calcium homeostasis. FAD-PS–dependent calcium alterations in intracellular calcium stores have been linked to synaptic dysfunction, which is the underlying basis for cognitive impairment in AD.[24] Screening of 20,000 small molecules using the HTS assay yielded the discovery of 52 primary hits, from which 4 lead structures were identified that belonged to the classes of compounds: thiazolidine, phenothiazine, imidazole, and benzhydrilpiperidinamine. Notably, existing evidence supports the beneficial effects of phenothiazine and thiazolidine derivatives for treatment of AD.[25–27] Such indications validate the relevance of this phenotypic screening strategy as well as the lead structures identified from it.

Alterations in intracellular calcium homeostasis can directly affect Aβ production.[6] Indeed, many of the active compounds identified from the primary calcium screen either increased or decreased the production of Aβ peptides. Such a broad range of effects on Aβ generation is most likely caused by targeting different components of intracellular calcium homeostasis by different hits. Indeed, calcium ions have been shown to directly regulate the activity of secretases.[28,29]

As it is typical for phenotypic drug screening approaches, the molecular targets of these hits are yet to be determined. However, we speculate that, some of the hits may dampen the hyperactivated calcium channels located on the ER,[15,21] modulate the PS holoprotein passive calcium leak channel activity,[20] or target the upstream elements involved in IP_3R-evoked calcium release,[15–17,19] thereby normalizing the disturbed ER calcium homeostasis.

Acknowledgments

Declaration of Conflicting Interests

Funding

References

1. Holtzman, D. M.; Morris, J. C.; Goate, A. M. Alzheimer's Disease: The Challenge of the Second Century. *Sci. Transl. Med*. **2011**, *3*, 77sr71.
2. Camandola, S.; Mattson, M. P. Aberrant Subcellular Neuronal Calcium Regulation in Aging and Alzheimer's Disease. *Biochim. Biophys. Acta* **2011**, *1813*, 965–973.
3. Honarnejad, K.; Herms, J. Presenilins: Role in Calcium Homeostasis. *Int. J. Biochem. Cell Biol*. **2012**, *44*, 1983–1986.
4. Stutzmann, G. E. The Pathogenesis of Alzheimers Disease: Is It a Lifelong "Calciumopathy"? *Neuroscientist* **2007**, *13*, 546–559.
5. Stutzmann, G. E.; Mattson, M. P. Endoplasmic Reticulum Ca^{2+} Handling in Excitable Cells in Health and Disease. *Pharmacol. Rev*. **2011**, *63*, 700–727.
6. Green, K. N.; LaFerla, F. M. Linking Calcium to Abeta and Alzheimer's Disease. *Neuron* **2008**, *59*, 190–194.
7. Pierrot, N.; Santos, S. F.; Feyt, C.; et al. Calcium-Mediated Transient Phosphorylation of Tau and Amyloid Precursor Protein Followed by Intraneuronal Amyloid-Beta Accumulation. *J. Biol. Chem*. **2006**, *281*, 39907–39914.
8. Coleman, P. D.; Yao, P. J. Synaptic Slaughter in Alzheimer's Disease. *Neurobiol. Aging* **2003**, *24*, 1023–1027.
9. Gomez-Isla, T.; Price, J. L.; McKeel, D. W., Jr.; et al. Profound Loss of Layer II Entorhinal Cortex Neurons Occurs in Very Mild Alzheimer's Disease. *J. Neurosci*. **1996**, *16*, 4491–4500.
10. Honarnejad, K.; Jung, C. K.; Lammich, S.; et al. Involvement of Presenilin Holoprotein Upregulation in Calcium Dyshomeostasis of Alzheimer's Disease. *J. Cell Mol. Med*. **2013**, *17*, 293–302.
11. Nagai, T.; Yamada, S.; Tominaga, T.; et al. Expanded Dynamic Range of Fluorescent Indicators for Ca^{2+} by Circularly Permuted Yellow Fluorescent Proteins. *Proc. Natl. Acad. Sci. U. S. A*. **2004**, *101*, 10554–10559.
12. Page, R. M.; Baumann, K.; Tomioka, M.; et al. Generation of Abeta38 and Abeta42 Is Independently and Differentially Affected by Familial Alzheimer Disease–Associated Presenilin Mutations and Gamma-Secretase Modulation. *J. Biol. Chem*. **2008**, *283*, 677–683.
13. Lipinski, C. A.; Lombardo, F.; Dominy, B. W.; et al. Experimental and Computational Approaches to Estimate Solubility and Permeability in Drug Discovery and Development Settings. *Adv. Drug Deliv. Rev*. **2001**, *46*, 3–26.
14. Carmichael, J.; DeGraff, W. G.; Gazdar, A. F.; et al. Evaluation of A Tetrazolium-Based Semiautomated Colorimetric Assay: Assessment of Chemosensitivity Testing. *Cancer Res*. **1987**, *47*, 936–942.
15. Cheung, K. H.; Shineman, D.; Muller, M.; et al. Mechanism of Ca^{2+} Disruption in Alzheimer's Disease by Presenilin Regulation of $InsP_3$ Receptor Channel Gating. *Neuron* **2008**, *58*, 871–883.
16. Thathiah, A.; De Strooper, B. The Role of G Protein–Coupled Receptors in the Pathology of Alzheimer's Disease. *Nat. Rev. Neurosci*. **2011**, *12*, 73–87.

17. Clader, J. W.; Wang, Y. Muscarinic Receptor Agonists and Antagonists in the Treatment of Alzheimer's Disease. *Curr. Pharm. Des*. **2005**, *11*, 3353–3361.

18. Tsang, S. W.; Lai, M. K.; Kirvell, S.; et al. Impaired Coupling of Muscarinic M1 Receptors to G-Proteins in the Neocortex Is Associated with Severity of Dementia in Alzheimer's Disease. *Neurobiol. Aging* **2006**, *27*, 1216–1223.

19. Cedazo-Minguez, A.; Popescu, B. O.; Ankarcrona, M.; et al. The Presenilin 1 deltaE9 Mutation Gives Enhanced Basal Phospholipase C Activity and a Resultant Increase in Intracellular Calcium Concentrations. *J. Biol. Chem*. **2002**, *277*, 36646–36655.

20. Tu, H.; Nelson, O.; Bezprozvanny, A.; et al. Presenilins Form ER Ca^{2+} Leak Channels, a Function Disrupted by Familial Alzheimer's Disease–Linked Mutations. *Cell* **2006**, *126*, 981–993.

21. Stutzmann, G. E.; Smith, I.; Caccamo, A.; et al. Enhanced Ryanodine Receptor Recruitment Contributes to Ca^{2+} Disruptions in Young, Adult, and Aged Alzheimer's Disease Mice. *J. Neurosci*. **2006**, *26*, 5180–5189.

22. Green, K. N.; Demuro, A.; Akbari, Y.; et al. SERCA Pump Activity Is Physiologically Regulated by Presenilin and Regulates Amyloid Beta Production. *J. Cell Biol*. **2008**, *181*, 1107–1116.

23. Herms, J.; Schneider, I.; Dewachter, I.; et al. Capacitive Calcium Entry Is Directly Attenuated by Mutant Presenilin-1, Independent of the Expression of the Amyloid Precursor Protein. *J. Biol. Chem*. **2003**, *278*, 2484–2489.

24. Ho, A.; Shen, J. Presenilins in Synaptic Function and Disease. *Trends Mol. Med*. **2011**, *17*, 617–624.

25. Akoury, E.; Pickhardt, M.; Gajda, M.; et al. Mechanistic Basis of Phenothiazine-Driven Inhibition of Tau Aggregation. *Angewandte Chemie* **2013**, *52*, 3511–3515.

26. Bulic, B.; Pickhardt, M.; Mandelkow, E. M.; et al. Tau Protein and Tau Aggregation Inhibitors. *Neuropharmacology* **2010**, *59*, 276–289.

27. Darvesh, S.; Macdonald, I. R.; Martin, E. Selectivity of Phenothiazine Cholinesterase Inhibitors for Neurotransmitter Systems. *Bioorg. Med. Chem. Lett*. **2013**, *23*, 3822–3825.

28. Hayley, M.; Perspicace, S.; Schulthess, T.; et al. Calcium Enhances the Proteolytic Activity of BACE1: An In Vitro Biophysical and Biochemical Characterization of the BACE1-Calcium Interaction. *Biochim. Biophys. Acta* **2009**, *1788*, 1933–1938.

29. Ho, M.; Hoke, D. E.; Chua, Y. J.; et al. Effect of Metal Chelators on Gamma-Secretase Indicates That Calcium and Magnesium Ions Facilitate Cleavage of Alzheimer Amyloid Precursor Substrate. *Int. J. Alzheimers Dis*. **2011**, *2011*, 950932.